EPJ Appl. Metamat. **7**, 2 (2020)

https://doi.org/10.1051/epjam/2020003

EPJ Applied Metamaterials

Available online at:
epjam.edp-open.org

Metamaterial Research Updates from China

RESEARCH ARTICLE OPEN ACCESS

Ultrathin polarization-insensitive tri-band THz perfect metamaterial absorber

Zhaomei Liu[1,*], Xingxing Han[1], and Aixia Wang[2]

[1] Xi'an Jiaotong University City College, Xi'an, PR China
[2] Department of Basic Sciences, Air Force Engineering University, Xi'an, PR China

Received: 1 July 2020 / Accepted: 30 July 2020

Abstract. In this paper, an ultrathin and polarization-insensitive THz perfect metamaterial absorber (PMA) was proposed using the traditional sandwiched structure with circular patch resonators on the top layer. The simulated spectrum shows that the proposed PMA has three distinctive absorption peaks at $f_1 = 0.8$ THz, $f_2 = 2.28$ THz and $f_3 = 3.62$ THz, with absorbance of 96.7%, 97.9% and 99.8%, respectively. The electric field distributions of the PMA reveal that the absorption mainly originates from the standing wave resonances between the top and bottom layers. The proposed PMA is polarization insensitive due to its axisymmetric unit cell structure. By adjusting the structure parameters, the resonance frequency, intensity and Q-factor of absorption peak can be tuned effectively. Our design may find potential applications in THz imaging, sensing and signal detection.

Keywords: Perfect metamaterial absorber (PMA) / circular patch resonator / the standing wave resonance theory

1 Introduction

Metamaterials have attracted much attention due to their unique electromagnetic properties which are unavailable in natural materials. Design perfect metamaterial absorbers (PMA) is an important point, which can achieve near unity absorption and has potential applications in sensing, stealth, detection and spectrum identification. A typical PMA consists of three layers in which the top metal unit structure layer, the middle dielectric spacer and the bottom opaque metal plate layer. The absorption frequency and intensity can be tuned by adjusting the shape and size of metal unit structure, the thickness and properties of dielectric spacer [1,2]. So far, the PMA with multi-band absorption [3–14], broadband absorption [15–19], controllable band absorption [20–22], polarization-insensitive and wide-angle absorption [23–27] have been reported in microwave, THz, infrared and visible bands. In order to meet the practical application requirements, the PMA should realize the strong absorption of electromagnetic waves in the wide frequency range under the premise of thin thickness and light weight. Multi-layer structure and non-planar structure are effective methods to achieve broadband absorption. However, these two means may increase the sample thickness and difficulties for fabrication. Broadband absorption could be achieved through multi-band absorption by meticulously adjustting the geometric parameters of the unit structure [28]. Design of broadband or multi-band PMAs using a simple polarization-insensitive structure with ultrathin thickness is still lacking in sufficient research progress.

In this work, an ultra-thin and polarization-insensitive THz PMA with circular patch resonators was designed. Perfect absorption at frequencies of $f_1 = 0.8$ THz, $f_2 = 2.28$ THz and $f_3 = 3.62$ THz is realized through carefully optimizing parameters of the structure. We investigated the electric field distributions and used the standing wave resonance theory to expound the absorption mechanism. Our absorber is polarization insensitive because of its axisymmetric unit structure. We also studied the influence of structure parameters on resonance frequency, intensity and quality factor. The proposed absorber has the simplest structure solving the problems of large unit size and fabrication difficulties. The proposed PMA would provide an operation to select the absorption frequency at terahertz band, and bring some potential applications.

2 Design, simulation results and discussion

Figure 1a shows the design schematic of the proposed PMA, which consists of Al circular patch, lossy silicon dielectric layer and Al ground plane. The front view of unit

* e-mail: lmhome@163.com

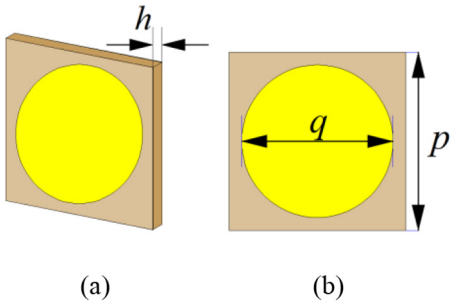

Fig. 1. The schematic of the unit cell of the proposed PMA. (a) Perspective view; (b) front view.

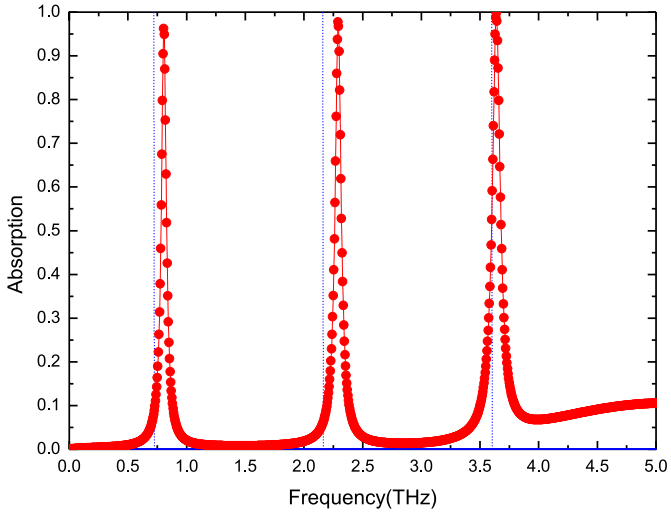

Fig. 2. Simulated absorption spectra induced by incident EM waves.

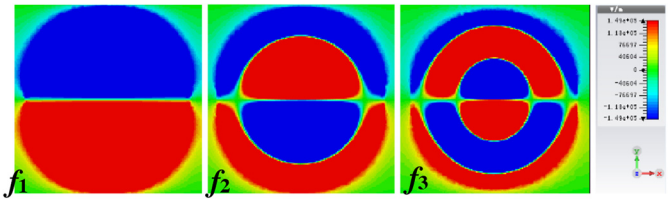

Fig. 3. Electric field component E_z at $z = 3.62\,\mu m$ corresponding to different absorption peaks when the phase is zero.

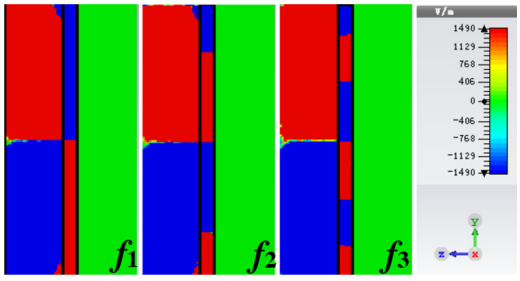

Fig. 4. Electric field component E_z at $x = 0$ corresponding to different absorption peaks when the phase is zero.

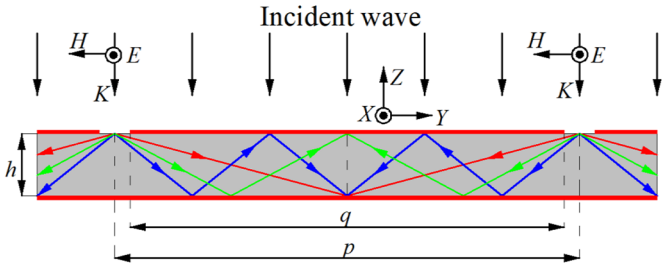

Fig. 5. The schematic diagram of the standing wave model.

cell is shown in Figure 1b. The optimized circular patch diameter $q = 60\,\mu m$, the periodic unit size $p = 70\,\mu m$, the Si spacer layer thickness $h = 3.6\,\mu m$ and dielectric constant $\varepsilon = 11.9$. The conductivity of Al is $3.56 \times 10^7\,S/m$. The thickness of metal layer is set as $0.2\,\mu m$ to ensure that no electromagnetic (EW) waves can pass through.

The electromagnetic response of the structure is simulated by the CST Microwave Studio software. The absorption spectra of EM waves is shown in Figure 2. It shows that there are three perfect absorption peaks at frequencies of $f_1 = 0.8\,THz$, $f_2 = 2.28\,THz$ and $f_3 = 3.62\,THz$, with absorbance of 96.7%, 97.9% and 99.8%, respectively.

To understand the absorption mechanism, we investigated the z component of the electric field distribution (E_Z) from f_1 to f_3 at each frequency. Figure 3 shows the E_Z distribution at the plane $z = 3.62\,\mu m$, which is the interface of dielectric and top metallic layer. As can be seen from Figure 3, the E-field is limited to local regions, with some regions being the strongest and some regions being zero. The electric field intensity on both sides of the unit cell center is always out of phase, and any side is always in phase, as shown in Figure 3a. The pattern of the E-field distribution is similar to the standing wave resonance pattern, Which is a typical model of a standing wave system with two ends open and the middle fixed.

The proposed PMA can be considered as a planar metal-insulator-metal wave guide. The gaps between the adjacent unit cells are smaller than the incident wave length. Electromagnetic waves diffract into dielectric layer through the gaps, then are reflected by the ground metal layer, as shown in Figure 5. If the absorber is thin enough, the EM waves from adjacent gaps may interference and form standing waves in y or x direction. Each unit cell is considered as a planar wave guide of a definite length L with both ends open, and the standing wave must have antinodes at both ends of the unit cell. Because of symmetric structure and the open boundary conditions, the center of unit cell is usually a node. Therefore, the possible standing wave mode can only be fundamental mode and its odd harmonic modes. The standing waves dissipate gradually in the lossy dielectric layer, and the corresponding antinodes are the locations of maximum loss energy densities. The resonance frequency of fundamental standing wave can be estimated by the following formula [3]:

$$f = \frac{c}{2nL} \tag{1}$$

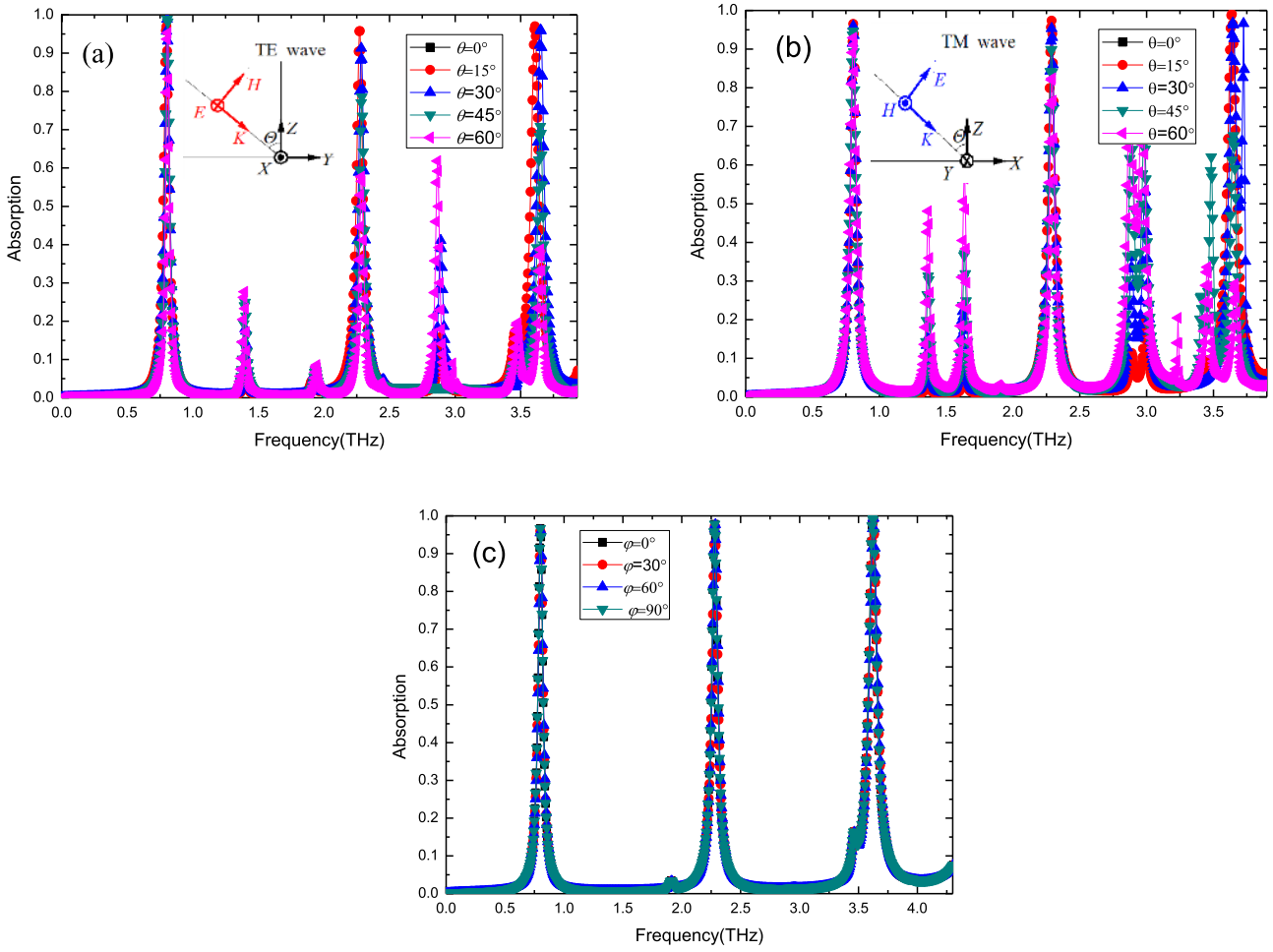

Fig. 6. Absorption spectra at different incident angles for (a) TE and (b) TM waves, when the azimuthal angle is fixed to $\varphi = 0°$. (c) Absorption spectra at different polarization angles when the incident angle is fixed to $\theta = 0°$.

where $c = 3 \times 10^8$ m $\times$ s^{-1} is the speed of light in vacuum, $n = \sqrt{\varepsilon_r} = \sqrt{11.9}$ is the refractive index of the lossy silicon and L is the length of the resonator. Taking the length $L = 60\,\mu$m into equation (1), we find the fundamental standing wave mode is 0.72 THz, the 3rd and 5th harmonic modes are 2.16 THz and 3.60 THz, which matching well with the simulation results, displayed by dashed blue lines in Figure 2. The slight difference is because that the real wave guide length is larger than the size of the top metal cell.

We further investigated the E_Z distribution in the yoz plane ($x = 0$), as shown in Figure 4. As can be seen, from f_1 to f_3, that the typical fundamental standing wave mode, and its 3rd, 5th harmonic modes are presented, respectively.

3 Absorption characteristics and analysis

Wide-angle stability and polarization insensitivity are the two key features of PMA. Therefore, we simulated the absorption at different incident angles for both the TE and TM polarizations. For TE polarization, only the absorption of f_2 is reducing slightly when the incident angle up to 30°, the absorption of f_2 and f_3 is reducing significantly with the angle up to 45°, the absorption of f_1 remains 95% with the angle up to 60°, as shown in Figure 6a. For TM polarization, the absorption peak f_3 splits into two separated absorption spectra when the incident angle up to 30°, the absorption of f_1 and f_2 remains 90% with the angle up to 45°, the absorption of f_1 is over 90% with the angle up to 60°, as shown in Figure 6b. As the incident angle increases, some new peaks appear. This may be because as the incident angle increases, the z component of the electric field increases, producing some additional resonance. Figure 6c shows that the absorption spectra does not change at different polarization angles, this due to the axisymmetric structure of the resonance unit cell. This indicates that the proposed PMA is insensitive to polarization. This characteristics is very important in practical applications.

Next, we studied the effect of structural geometry parameters on absorption characteristics. Figure 7a shows the influence of dielectric thickness h, and all three absorption peaks move towards low-frequency direction slightly with the increase of h. It can be seen that the fundamental standing wave mode absorption peak (f_1) is insensitive to the dielectric thickness h. As the circular

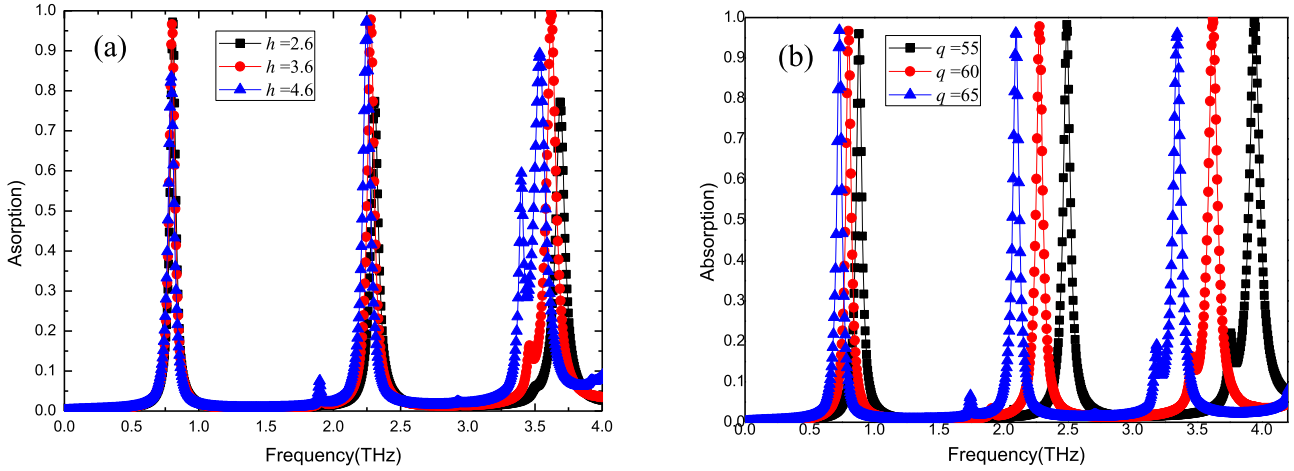

Fig. 7. The influence of structural parameters on the absorption. (a) Change dielectric thickness h, (b) change circular patch diameter q, where other parameters remains unchanged.

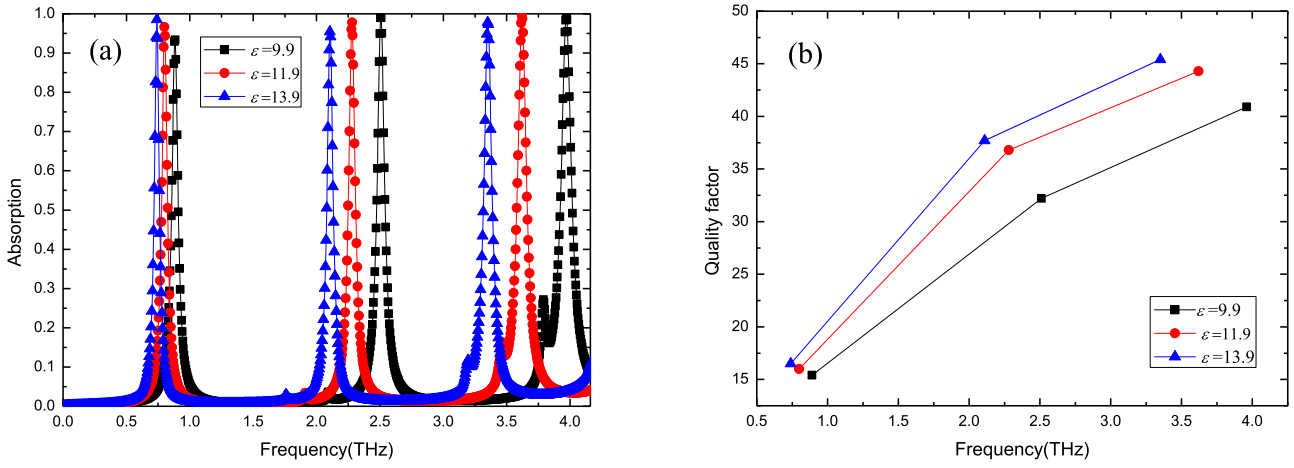

Fig. 8. The impact of dielectric constant ε on the (a) absorption; (b) quality factor.

patch diameter q changes from 55 to 65 μm, all absorption peaks shift towards the lower frequencies with the increase of q, as shown in Figure 7b. It is clear that the magnitudes of the three absorption peaks almost unchanged with the increase of q.

Finally, we investigated the impact of the dielectric constant ε on the quality factor (Q-factor). Figure 8a shows the influence of ε, three absorption peaks move towards lower frequencies with the increase of ε, this is consistent with equation (1). As can be seen from Figure 8b, the Q-factor becomes larger with dielectric constant ε increasing, and the higher the standing wave mode is, the higher the Q-factor is. Obviously, higher order resonance modes can improve the Q-factor. Therefore, the proposed PMA will be usefull in sensing applications, where higher order resonance mode can be used [29,30].

4 Conclusions

In conclusion, an ultrathin and polarization insensitive THz PMA is proposed, with circular patch resonators in the top layer. The proposed PMA has three perfect absorption peaks at $f_1 = 0.8$ THz, $f_2 = 2.28$ THz and $f_3 = 3.62$ THz, with absorbance of 96.7%, 97.9% and 99.8%, respectively. The absorption of the proposed PMA was unchanged for all polarization angles. The total thickness of the proposed PMA is only 4.0 μm, which is about $\lambda/36$ at 2.28 THz. The simulated electric field distributions indicate that three perfect absorption peaks mainly originated from the fundamental standing wave mode, its 3rd and 5th harmonic modes. By adjusting the structure parameters, the resonance frequency, intensity and the Q-factor of the absorption peaks can be tuned effectively. Our design would have some potential applications in detection, sensing and stealth.

References

1. N.I. Landy, S. Sajuyigbe, J.J. Mock, D.R. Smith, W.J. Padilla, Phys. Rev. Lett. **100**, 207402 (2008)
2. C.M. Watts, X. Liu, W.J. Padilla, Adv. Mater. **24**, 98–120 (2012)
3. X.Y. Peng, B. Wang, S.M. Lai, D.H. Zhang, J.H. Teng, Opt. Express **20**, 27756–27765 (2012)

4. F.R. Hu, L. Wang, B.G. Quan, X.L. Xu, Z. Li, Z.A. Wu, X.C. Pan, J. Phys. D: Appl. Phys. **46**, 195103 (2013)
5. W.J. Wang, M.B. Yan, Y.Q. Pang, J.F. Wang, H. Ma, S.B. Qu, H.Y. Chen, C.L. Xu, M.D. Feng, Appl. Phys. A **118**, 443–447 (2015)
6. D. Hu, H.Y. Wang, Q.F. Zhu, IEEE Photon. J. **8**, 5500608 (2016)
7. K. Kumari, N. Mishra, R.K. Chaudhary, Microw. Opt. Technol. Lett. **59**, 2664–2669 (2017)
8. M.M. Hasan, M.R.I. Faruque, M.T. Islam, Opt. Technol. Lett. **59**, 2302–2307 (2017)
9. X.F. Su, G.H. Li, H. Yang, Z.Y. Zhao, X.S. Chen, W. Lu, Plasmonics **13**, 729–735 (2018)
10. T.H. Meng, D. Hu, Q.F. Zhu, Opt. Commun. **415**, 151–155 (2018)
11. B.X. Wang, G.Z. Wang, Plasmonics **13**, 123–130 (2018)
12. N. Mishra, K. Kumari, R.K. Chaudhary, Int. J. Microw. Wirel. Technol. **10**, 422–429 (2018)
13. S. Kalraiya, R.K. Chaudhary, R.K. Gangwar, M.A. Abdalla, Mater. Res. Express **6**, 055812 (2019)
14. A.X. Wang, S.B. Qu, M. Yan et al., Appl. Phys. A **125**, 331 (2019)
15. J.F. Zhu, Z.F. Ma, W.J. Sun, F. Ding, Q. He, L. Zhou, Y.G. Ma, Appl. Phys. Lett. **105**, 021102 (2014)
16. X.J. He, S.T. Yan, Q.X. Ma, Q.F. Zhang, P. Jia, F.M. Wu, J. X. Jiang, Opt. Commun. **340**, 44–49 (2015)
17. T. Liu, S.S. Kimn, Opt. Commun. **359**, 372–377 (2016)
18. R.X. Deng, M.L. Li, B. Muneer, Q. Zhu, Z.Y. Shi, L.X. Song, T. Zhang, Materials **11**, 107 (2018)
19. M.D. Banadaki, A.A. Heidari, M. Nakhkash, IEEE Antennas and Wireless Propagation Letters **17**, 205–208 (2018)
20. H.Y. Zheng, X.R. Jin, J.W. Park, Y.H. Lu, J.Y. Rhee, W.H. Jang, H. Cheong, Y.P. Lee, Opt. Express **20**, 24002–24009 (2012)
21. P.V. Tuong, J.W. Park, J.Y. Rhee, K.W. Kim, W.H. Jang, H. Cheong, Y.P. Lee, Appl. Phys. Lett. **102**, 081122 (2013)
22. X.G. Zhao, K. Fan, J.D. Zhang, G.R. Keiser, G.W. Duan. R.D. Averitt, X. Zhang, Microsyst. Nanoeng. **2**, 16025 (2016)
23. B. Zhang, Y. Zhao, Q. Hao, B. Kiraly, I.C. Khoo, S. Chen, T. J. Huang, Opt. Express **19**, 15221–15228 (2011)
24. Y.J. Yoo, Y.J. Kim, T.P. Van, J.Y. Rhee, K.W. Kim, W.H. Jang, Y.H. Kim, H. Cheong, Y.P. Lee, Opt. Express **21**, 32484–32490 (2013)
25. J.Y. Tang, Z.Y. Xiao, K.K. Xu, X.L. Ma, Z.H. Wang, Plasmonics **11**, 1393–1399 (2016)
26. L.Y. Guo, X.H. Ma, Y.G. Zou, R.B. Zhang, J.A. Wang, D. Zhang, Opt. Laser. Tech. **98**, 247–251 (2018)
27. R. Asghariana, B. Zakeria, O. Karimib, Int. J. Electron. Commun. (AEÜ) **87**, 119–123 (2018)
28. J.Y. Rhee, Y.J. Yoo, K.W. Kim, Y.J. Kim, Y.P. Lee, J. Electromag. Waves Appl. **28**, 1541–1580 (2014)
29. M. Wu, X.G. Zhao, J.D. Zhang, J. Schalch, G.W. Duan, K. Cremin, R.D. Averitt, X. Zhang, Appl. Phys. Lett. **111**, 051101 (2017)
30. G.W. Duan, J. Schalchb, X.G. Zhao, J.D. Zhang, R.D. Averitt, X. Zhang, Sensor. Actuat. A **280**, 303–308 (2018)

Cite this article as: Zhaomei Liu, Xingxing Han, Aixia Wang, Ultrathin polarization-insensitive tri-band THz perfect metamaterial absorber, EPJ Appl. Metamat. **7**, 2 (2020)